# Proposal and applications of a method for the study of irreversible phase transitions

Ernesto S. Loscar, Nara Guisoni, and Ezequiel V. Albano
*Instituto de Investigaciones Fisicoquímicas Teóricas y Aplicadas (INIFTA), CCT-La Plata CONICET, Facultad de Ciencias Exactas, Universidad Nacional de La Plata, Sucursal 4, CC 16, 1900 La Plata, Argentina*
(Received 4 September 2009; revised manuscript received 26 October 2009; published 23 November 2009)

The gradient method for the study of irreversible phase transitions in far-from-equilibrium lattice systems is proposed and successfully applied to both the archetypical case of the Ziff-Gulari-Barshad model [R. M. Ziff *et al.*, Phys. Rev. Lett. **56**, 2553 (1986)] and a forest-fire cellular automaton. By setting a gradient of the control parameter along one axis of the lattice, one can simultaneously treat both the active and the inactive phases of the system. In this way different interfaces are defined whose study allows us to find the active-inactive phase transition (both of first and second order), as well as the description of the active phase as composed of two further phases: the percolating and the nonpercolating ones. The average location and the width of the interfaces obey standard scaling behavior that is essentially governed by the roughness exponent $\alpha=1/(1+\nu)$, where $\nu$ is the suitable correlation length exponent.

DOI: 10.1103/PhysRevE.80.051123 PACS number(s): 05.70.Fh, 02.50.−r, 64.60.ah, 82.20.Wt

## I. INTRODUCTION

Irreversible phase transitions (IPTs) in far-from-equilibrium systems take place between an active (or reactive) state and an inactive (or absorbing) regime, such that the system becomes irreversibly trapped into the absorbing phase when a suitable control parameter is finely tuned across the transition point. The study and understanding of IPTs not only have attracted considerable attention in the field of nonequilibrium statistical physics, but they are also topics of interdisciplinary interest. In fact, IPTs have been reported in models for heterogeneously catalyzed reactions, epidemic spreading, forest-fire (FF) propagation, prey-predator competition, various cellular automata aimed to mimic biological systems, etc. [1–3]. In spite of the fact that second- and first-order IPTs share many properties with their equilibrium counterparts, one often needs to develop new methods and approaches in order to treat them. In fact, since large fluctuations close to criticality may drive the system to an absorbing state, finite-size scaling methods may not be so useful for the study of second-order IPTs. Instead, the so-called "epidemic method" has become the most popular tool for this kind of study [1,2,4]. Furthermore, in order to deeply study first-order IPTs, both the stationary [5] and the driven [6] constant coverage ensembles have been developed, which allows for the precise determination of the coexistence point and the spinodals, and also recording hysteretic effects [7].

On the other hand, the standard percolation problem [8], which is the archetypical model for a geometrical critical phenomena studied in the field of statistical physics, can also be studied by considering the density gradient of diffusing particles that is generated between a source and a sink. In fact, that approach originates the so-called gradient percolation method that is the generalization of the early pioneer work of Sapoval *et al.* [9]. Subsequently, this method has been applied not only to the theoretical study of different physical problems such as the overlapping disks in a concentration gradient [10], bond percolation for the Kagome lattice [11], but also to analyze some experimental situations where concentration gradients are present, as, e.g., invasion percolation under gravity (see references in the review [12]), porous media [13], and in the study of vegetation distribution [14]. In all these cases, the gradient percolation method is used to study the percolation transition, through the localization of an interface between a percolating and a nonpercolating phase, which for the case of an infinite lattice size corresponds to the hull of the incipient percolation cluster. Related versions of the gradient percolation method are the hull-gradient method [15] and the illumination method [16].

Within this broad context, the aim of this paper is to propose an alternative approach for the study of IPTs, namely the gradient method (GM). Inspired in the gradient percolation method, by setting a gradient in the control parameter we are able to study both the percolation transition and all type IPTs (of both first and second order), in a unified fashion.

Along this work we present a successfully implementation of the GM in two far-from-equilibrium models: an archetypical model for catalytic reactions, the Ziff-Gulari-Barshad (ZGB) model [17] (Sec. II A), and a forest-fire cellular automaton model with immunity [18] (Sec. II B). We state our conclusions in Sec. III.

## II. APPLICATIONS OF THE GM

### A. ZGB gradient model

The ZGB [17] is a model for the catalytic oxidation of CO, which proceeds according to the Langmuir-Hinshelwood mechanism, i.e., with the reactants adsorbed on the surface of the catalyst, namely,

$$\mathrm{CO}(g) + \mathrm{S} \rightarrow \mathrm{CO}(a), \tag{1}$$

$$\mathrm{O_2}(g) + 2\mathrm{S} \rightarrow 2\mathrm{O}(a), \tag{2}$$

$$\mathrm{CO}(a) + \mathrm{O}(a) \rightarrow \mathrm{CO_2}(g) + 2\mathrm{S}, \tag{3}$$

where $(a)$ and $(g)$ refer to the adsorbed and gas phases, respectively. CO adsorption [Eq. (1)] takes place, with prob-

 

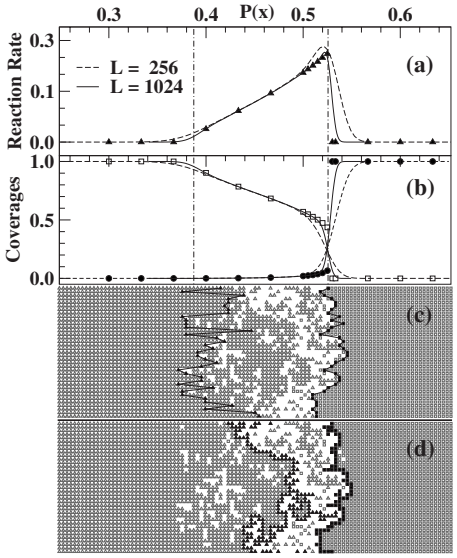


FIG. 1. (a) Rate of $CO_2$ production ($R_{CO_2}$) and (b) coverages of the adsorbed reactants CO ($\theta_{CO}$) and $O$ ($\theta_{OX}$), versus the pressure of CO ($P$). Continuous and dashed lines are results obtained by means of the GM with the indicated lattice sizes. Symbols (▲ for $R_{CO_2}$, ● for $\theta_{CO}$, and □ for $\theta_{OX}$) are extrapolated results from standard simulations. Vertical lines show the values of $P_1$ (left) and $P_2$ (right). For the sake of clarity, (c) and (d) show the same snapshot configuration obtained during a simulation with the GM ($L_x$ =256). Triangles and squares are used for adsorbed O and CO, respectively, while empty sites are left in white. The filled symbols represent the sites belonging to the SVI (c) and MVI (d), respectively, and are connected by solid lines in order to guide the eyes.

ability $P_{CO}$, at a single site $S$, while $O_2$ adsorption, which occurs with probability $P_{O_2}$, requires a pair of neighboring sites [Eq. (2)]. The desorption of $CO_2$ [Eq. (3)] vacates two sites of the surface. By normalizing the partial pressures of the reactants, i.e., $P_{CO}+P_{O_2}=1$, the model can be handled with a single parameter given by $P_{CO}\equiv P$. Simulations of the ZGB model account for the catalyst surface by means of the square lattice. By using a standard procedure, independent simulations are performed for different values of the control parameter in order to draw the phase diagram, i.e., a plot of the surface density of the reactants ($\theta_{CO}$ and $\theta_{OX}$), as well as the rate of $CO_2$ production ($R_{CO_2}$), versus $P$. The ZGB exhibits a second-order IPT at $P_1 \cong 0.3874$ [19], and a first-order IPT at $P_2 \cong 0.5256$ [17]. For details on this model and the simulation methods used, see, e.g., [7].

Here, we propose the GM, such that the surface of the catalyst along the horizontal ($x$ direction) axis has a pressure given by $P(x)=(x/L_x)^k$, where $L_x$ is the horizontal lattice side, $1 \leq x \leq L_x$, and $k$ is an exponent. We have found that the results of the application of GM are independent on the vertical lattice side $L_y$ (with $L_x \leq L_y$). Also $k=1/2,1,2,3$ basically gives the same results, e.g., transition points and exponents, so that hereafter we focus on the case $k=1$ only, with the gradient $\Delta=1/L_x$. Of course, open and periodic boundary conditions are imposed along the $x$ and $y$ directions, respectively. Figures 1(a) and 1(b) show plots of the phase diagram of the ZGB model as obtained by means of a single simulation of the GM. We show plots of $R_{CO_2}(x)$, $\theta_{CO}(x)$, and $\theta_{OX}(x)$, versus $P(x)$ for lattices of different sides, which are compared with results from standard simulations. As can be seen in Figs. 1(a) and 1(b), when the size of the sample is increased the phase diagram of the ZGB model obtained by means of the GM tends to the (extrapolated) results corresponding to the standard method. Furthermore, Figs. 1(c) and 1(d) exhibit a useful feature of the GM: both the O- and CO-poisoned phases, as well as the reactive phase, can be observed simultaneously on the left-hand, middle, and right-hand sides of the snapshots, respectively.

In order to achieve a quantitative description of the interfaces shown in Figs. 1(c) and 1(d) we have used two definitions, and consequently two algorithms, to locate them. The simplest definition corresponds to a *single-valued interface* (SVI). For the case of the O-poisoned phase, the SVI is given by the set of points $\{x_j, j=1,\ldots,L_y\}$ belonging to the poisoned phase that are in contact with the active phase, but are located on the leftmost side of each arrow $j$ [shown on the left side of Fig. 1(c)]. Similarly, the SVI for the CO-poisoned phase is composed by the $L_y$ points belonging to the poisoned phase that are in contact with the active phase, but are located on the rightmost side of each arrow $j$ [shown on the right side of Fig. 1(c)]. The average pressure undergone by the sites belonging to the SVI is given by

$$P_X^{SVI} = \frac{1}{L_y}\sum_{j=1}^{L_y} P(x_j), \tag{4}$$

while its width is given by

$$w_X^{SVI} = \sqrt{\frac{1}{L_y}\sum_{j=1}^{L_y} [P(x_j) - P_X^{SVI}]^2}. \tag{5}$$

Here the subindex $X=OX$ (CO) refers to the interface of the massive O(CO) cluster.

On the other hand, if one considers connectivity between the particles a *multivalued interface* (MVI) can be obtained, as in the case of the gradient percolation method [9,12,14]. In order to construct the MVI for the gradient version of the ZGB model, we proceed as follow. For the case of O-poisoned phase one first determines all O-occupied sites in contact with the massive O-cluster located on the left of the sample [see Fig. 1(d)]. These sites, connected by means of nearest neighbors, are denoted as the "land." Empty and CO-occupied sites are linked through both nearest- and next-nearest-neighbor sites and form a large cluster that is termed the "sea." The sites not connected with the two large clusters of land and sea are identified as "islands" and "lakes," respectively, but they are irrelevant. In fact, the interface is given by the seashore where land and sea are in contact [9,14,20]. It is worth mentioning that the number of points belonging to the MVI ($N_{MVI}$) is greater than $L_y$, which motivates the name of the multivalued interface, in contrast to the single-valued interface. The above definition for the MVI can also be applied to the CO poisoned phase. But now by considering the CO-occupied sites in contact with the massive CO-cluster on the right side of the sample [see Fig. 1(d)] as the land, and both empty and O-occupied sites as the sea. Also, the average pressure of the MVI ($P_X^{MVI}$) and its width

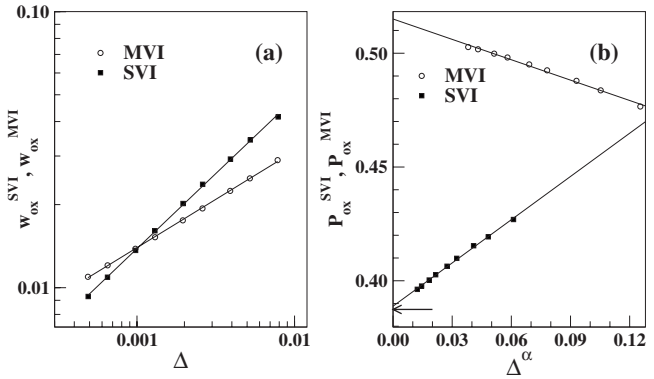


FIG. 2. (a) Log-log plot of the width $w$ of MVI (○) and SVI (■) versus the CO-pressure gradient Δ. (b) The mean pressure of MVI and SVI $[P_{ox}^{MVI}(\Delta),\ P_{ox}^{SVI}(\Delta)]$ versus $\Delta^{\alpha}$. Intersections with the $y$ axis represent the extrapolation to the zero gradient [see Eq. (9)]. The arrow indicates $P_1$. Error bars are smaller than the symbol size.

$(w_X^{MVI})$ can be evaluated as in the case of the SVI, but regarding the set of $N_{MVI}$ sites that compose the MVI. That means, considering $N_{MVI}$ instead of $L_y$ in Eqs. (4) and (5), for both $X=OX$ and $X=CO$.

According to the dynamic scaling theory for self-affine interfaces [21], the interface width measured in lattice units $(W_L)$ scales according to $W_L \propto L_y^{\alpha^*}$, where $\alpha^*$ is the roughness exponent and $L_y$ is the finite length along the direction parallel to the interface. However, as in the case of the diffusion front [20], the scaling behavior in the GM is dominated by the diverging correlation length along the direction perpendicular to the interface, i.e., the direction where the gradient is applied, $L_x$. Therefore in the GM one has that $W_L \propto L_x^{\alpha^*}$. If the interface width is measured in units of pressure $(w)$, as in the case of Eq. (5), one has that $w=(dP/dx)W_L$. Since $P(x)=(x/L_x)$, as defined before, one obtains $w=(1/L_x)W_L \propto L_x^{\alpha^*-1}$. Then, by defining $\alpha=1-\alpha^*$, one concludes that

$$w \propto L^{-\alpha} = \Delta^{\alpha}, \tag{6}$$

where $\alpha$ is the exponent as yielded by the GM, for the width measured in units of pressure.

Figure 2(a) shows that, in fact, log-log plots of both $w_{ox}^{SVI}$ and $w_{ox}^{MVI}$ versus the gradient are consistent with power-law dependences and the obtained exponents are $\alpha_{ox}^{SVI}=0.56(2)$ and $\alpha_{ox}^{MVI}=0.36(4)$.

In the work of Sapoval *et al.* [9] it has been shown that the diffusion front of noninteracting particles (except for the excluded volume) defines a self-affine interface which is related to the standard percolation problem. Let us now recall that the percolation transition is characterized by a diverging correlation length $\xi \propto |p-p_c|^{-\nu}$, where $\nu=4/3$ is the correlation length exponent, $p$ is the probability (or density of occupied sites), and $p_c$ is the critical threshold [8,9,22]. In this way, the width of the diffusion front scales according to $W_L \propto L^{\nu/(1+\nu)}$ [9]. Since we define the MVI exactly with the same rules that the self-affine interface of the diffusion front, we expected that this relationship should also hold for the MVI. So, according to our terminology $\alpha^*=\nu/(1+\nu)$, and using the relationship $\alpha=1-\alpha^*$, we obtain that

$$\alpha = \frac{1}{1+\nu}, \tag{7}$$

which for $\nu=4/3$ gives $\alpha=3/7\cong 0.4286$. Now, by considering that $P$ in the GM is analogous to the density gradient between the source and the sink in the diffusion problem, the obtained exponent $\alpha_{ox}^{MVI}=0.36(4)$ is consistent with the exact value [Eq. (7)]. The neighborhood of the percolation transition with the first-order coexistence point leads to the occurrence of interference effects that hinder a more accurate determination of $\alpha_{ox}^{MVI}$, at least for the lattice sides used in this paper. This effect is absent in the forest-fire model where one can evaluate the exponent more accurately (see below).

On the other hand, it has been shown that the location of the MVI in the gradient percolation provides an accurate value of the percolation threshold [23]. For the ZGB gradient model, the mean pressure of CO at both the MVI and the SVI [$P_X^{SVI}$, given by Eq. (4), and $P_X^{MVI}$, respectively] can be considered as estimations of the critical pressures for the corresponding transitions. In order to extrapolate $P_X^{SVI}$ and $P_X^{MVI}$ to the thermodynamic limit we recall the theory of the standard percolation problem. In this way, it is well known that the exponent of the threshold fluctuation can be used to extrapolate the critical density to the thermodynamic limit [8], that is

$$P(L) = P(L \to \infty) + AL^{-\nu}, \tag{8}$$

where $P(L\to\infty)$ is the extrapolated percolation threshold, $P(L)$ is an "effective" threshold as determined for a finite sample of side $L$, and $A$ is a constant. For the ZGB gradient model we propose a similar relationship for the mean pressures of CO at the interfaces (considering SVI and MVI, for both the massive CO cluster and the massive O cluster). In fact, by setting $L=L_x$, using the exponent of the pressure fluctuation $\alpha$ [given by Eq. (6)], and remembering that $\Delta=1/L_x$, one has that Eq. (8) becomes

$$P(\Delta) = P(\Delta \to 0) + A\Delta^{\alpha}. \tag{9}$$

Figure 2(b) shows plots of $P_{ox}^{SVI}(\Delta)$ and $P_{ox}^{MVI}(\Delta)$ versus $\Delta^{\alpha}$. The extrapolation of the MVI gives $P_{ox}^{MVI}=0.51(1)$, which is identified as the percolation threshold of the O-percolating cluster. The density of O at the location of the MVI is $\theta_{OX}=0.515(15)$, i.e., a figure much smaller than the corresponding value for random percolation of both monomers $(p_c\simeq 0.59)$ and dimers $(p_c\simeq 0.56)$, indicating that the reaction acts as an attractive effective interaction, in agreement with previous results [24]. Focusing our attention on the scaling behavior of the SVI, it follows that the extrapolation of Eq. (9) yields $P_{ox}^{SVI}=0.3880(8)$, in excellent agreement with the best available estimation of the critical point of the ZGB model given by $P_1=0.3874$ [19]. The fact that the properties of the SVI can be fitted with the same exponent $[\alpha_{ox}^{SVI}=0.56(2)]$ can be understood because the second-order IPT of this model belongs to the directed percolation universality class (in $d+1$ dimensions, with $d=2$), so one can argue as in the case of standard percolation, but considering that now the (spatial) correlation length diverges as $\xi \propto |p-p_c|^{-\nu_\perp}$ (here $p\equiv P$) and $\nu_\perp=0.733(4)$ [1–3]. Then, by replacing $\nu_\perp$ in Eq. (7) one gets $\alpha_{ox}^{SVI}=0.577$, in excellent

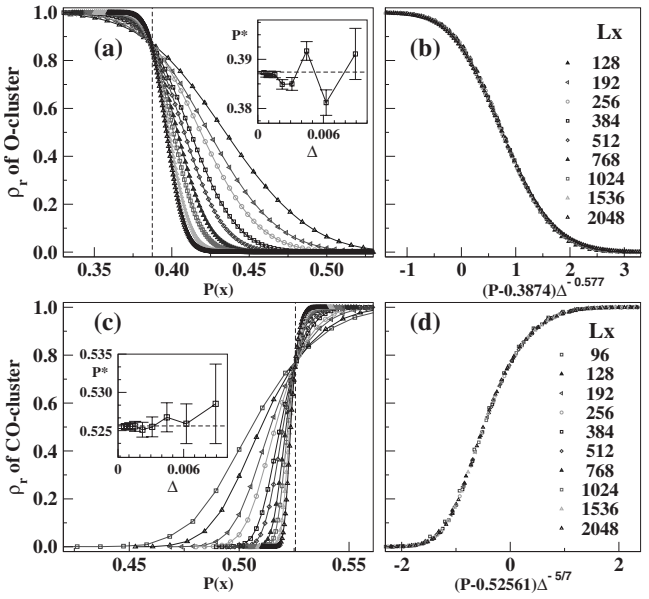


FIG. 3. (a) and (c) Plots of the relative density $\rho_r$ profile of the poisoning O and CO clusters, respectively, evaluated up to the SVI versus $P$, as obtained for samples of different side. The insets show the dependence of the intersection point $P^*$, between curves for consecutive gradients ($\Delta_1$ and $\Delta_2$) on $(\Delta_1+\Delta_2)/2$. Vertical dashed lines show the values of the transitions points. (b) and (d) Scaled plots of the data shown in (a) and (c), respectively. More details in the text.

agreement with the exponent obtained for the SVI. Further valuable information can be obtained by computing the normalized density $[\rho_r(x)]$ of the inactive O-poisoned cluster relative to the total number of O atoms in each column, as shown in Fig. 3(a). Here one roughly observes a common intersection point ($P^*$) for all the profiles evaluated for different $L_x$ (i.e., different gradients). A more careful inspection allows us to calculate the intersection points between profiles of consecutive sizes, which extrapolate to the critical point $P_1$, as shown in the inset of Fig. 3(a). This behavior implies that one can obtain data collapse just by rescaling the horizontal axis by $(P-P_1)\Delta^{-\alpha_{ox}^{SVI}}$, as conclusively shown in Fig. 3(b).

For the case of the first-order IPT of the ZGB model, one has that the width of both the SVI and the MVI of the massive CO cluster scales with the same exponent $\alpha_{co}^{SVI}=\alpha_{co}^{MVI}=0.68(2)$ (data not shown here). On the other hand, by using Eq. (9) one has that both effective thresholds extrapolate to the same (coexistence) point given by $P_{co}^{SVI}=P_{co}^{MVI}=0.5253(5)$, in excellent agreement with previous determinations, e.g., $P_2=0.52561$ [5]. Also, plots of the normalized density profiles of the inactive CO cluster versus $P$, obtained for lattices of different $L_x$, show a behavior similar to that of the second-order transition as shown in Fig. 3(c). In the same way, the extrapolation of the intersection points tends to $P_2$, i.e., the coexistence point. Furthermore, as in the case of second-order IPT, one can obtain excellent data collapsing of the profiles just by scaling the horizontal axis [Fig. 3(d)]. In order to understand the measured exponents, $\alpha_{co}^{SVI}$ and $\alpha_{co}^{MVI}$, we remind the reader that due to the absence of a diverging

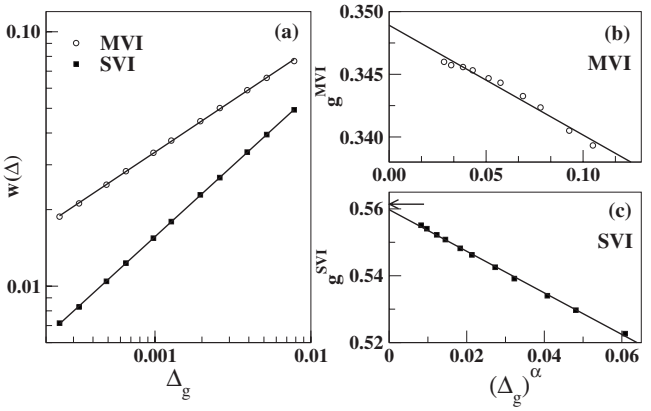


FIG. 4. Results for the FF model with immunity for $p=0.5$. (a) Log-log plots of the width $w$ of the MVI (○) and the SVI (■) versus the immunity gradient $\Delta_g$. (b) and (c) show the mean immunity of the MVI and the SVI ($g^{MVI}$ and $g^{SVI}$, respectively) versus $(\Delta_g)^\alpha$. Error bars are smaller than the symbol size. Intersections with the vertical axis give the percolation threshold for the case of the MVI (b) and the critical point for the SVI (c). The arrow indicates $g_c$ as obtained by means of the epidemic method [26].

correlation length in the first-order transition, one has that the overall behavior is dominated by the divergence of the correlation length of the self-affine interface of the massive CO cluster that belongs to the Kardar-Parisi-Zhang (KPZ) universality class [25], with $\nu_\perp=2/5$ [21], which inserted in Eq. (7) yields $\alpha=5/7\simeq 0.7143$, consistent with our fits.

### B. Forest-fire model in an immunity gradient

In the FF cellular automaton [18], each site of a lattice can be in three possible states: occupied by a tree, empty or occupied by a burning tree (fire). The trees grow at empty sites with probability $p$, healthy trees catch fire from adjacent burning trees with probability $(1-g)$, where $g$ is the immunity, and a burning tree becomes an empty site spontaneously. The standard simulation method shows that the FF presents a second-order IPT between an active phase and an absorbing phase [26], which belongs to the directed percolation universality class.

By using the GM in the FF, besides the usual active-absorbing transition of the model, one also finds the transition between the active-percolating and the active-nonpercolating phases [27]. The exponents for $p=0.5$, obtained from Fig. 4(a), are: $\alpha_{FF}^{MVI}=0.41(2)$ and $\alpha_{FF}^{SVI}=0.56(2)$, both in good agreement with Eq. (7) with $\nu=4/3$ and $\nu_\perp=0.733$, respectively. The extrapolations to the zero gradient shown in Figs. 4(b) and 4(c) give, respectively, the percolation threshold $g_p=0.349(3)$ and the critical point $g_c=0.560(1)$ (the latter in excellent agreement with previous result obtained by means of the epidemic method [26]). On the other hand, the threshold density of the green sites for the percolation transition is $\rho_{FF}\simeq 0.58$ [27], i.e., a figure close to the random percolation threshold.

## III. CONCLUSIONS

Summing up, the proposed GM for the study of IPTs allows us to simultaneously treat both second and first-order

transitions, in a unified fashion. Furthermore, with the SVIs we are able to determine the active-inactive transition (no matter the order of the transition), whereas the MVIs allow us to split up the active phase into two regimes: the percolating and the nonpercolating ones. The MVI at second-order IPTs captures the standard percolation features of the system, while the SVI is dominated by the directed percolation nature of the transition. In contrast, the abrupt first-order IPT of the ZGB model washes out the differences between these two types of interfaces that merge together into a KPZ behavior at coexistence. In this transition there is an abrupt change in the coverage of CO, which jumps from $\theta_{CO} \sim 0.07$, in the active phase, to $\theta_{CO}=1$, in the absorbing phase [see Fig. 1(b)]. Since the threshold of the percolation transition of random monomers is $\theta_{CO} \approx 0.59$, this transition is trapped in the active-absorbing transition. Therefore, for the first-order IPT of the ZGB model both the SVI and the MVI are completely equivalent.

For all the studied interfaces by means of the GM, the correlation length exponent ($\nu_\perp$ for directed percolation, $\nu$ for standard percolation and $\nu_\perp$ in the KPZ regime) dominates their scaling behavior through the exponent $\alpha=1/(1+\nu)$.

## ACKNOWLEDGMENTS

We acknowledge financial support from CONICET, ANPCyT, and UNLP (Argentina). We thank Claudio Horowitz for fruitful discussions about this work. We also acknowledge the anonymous referee that introduced us to the interesting work of M. T. Gastner *et al.*

[1] H. Hinrichsen, Adv. Phys. **49**, 815 (2000).
[2] G. Odor, Rev. Mod. Phys. **76**, 663 (2004).
[3] J. Marro and R. Dickman, *Nonequilibrium Phase Transitions and Critical Phenomena* (Cambridge University Press, Cambridge, England, 1999).
[4] P. Grassberger and A. de la Torre, Ann. Phys. (N.Y.) **122**, 373 (1979).
[5] R. M. Ziff and B. J. Brosilow, Phys. Rev. A **46**, 4630 (1992).
[6] E. S. Loscar and E. V. Albano, Comput. Phys. Commun. **180**, 488 (2009).
[7] E. S. Loscar and E. V. Albano, Rep. Prog. Phys. **66**, 1343 (2003).
[8] D. Stauffer and A. Aharoni, *Introduction to the Percolation Theory* (Taylor & Francis, Washington, DC, 1992).
[9] B. Sapoval, M. Rosso, and J. F. Gouyet, J. Phys. (Paris), Lett. **46**, L149 (1985).
[10] M. Rosso, J. Phys. A **22**, L131 (1989).
[11] R. M. Ziff and P. N. Suding, J. Phys. A **30**, 5351 (1997).
[12] J. F. Gouyet and M. Rosso, Physica A **357**, 86 (2005).
[13] M. Rosso, J. F. Gouyet, and B. Sapoval, Phys. Rev. Lett. **57**, 3195 (1986).
[14] M. T. Gastner, B. Oborny, D. K. Zimmermann, and G. Pruessner, Am. Nat. **174**, E23 (2009).
[15] R. M. Ziff and B. Sapoval, J. Phys. A **19**, L1169 (1986).
[16] A. Margolina and M. Rosso, J. Phys. A **25**, 3901 (1992).
[17] R. M. Ziff, E. Gulari, and Y. Barshad, Phys. Rev. Lett. **56**, 2553 (1986).
[18] B. Drossel and F. Schwabl, Physica A **199**, 183 (1993).
[19] C. A. Voigt and R. M. Ziff, Phys. Rev. E **56**, R6241 (1997).
[20] V. C. Chappa and E. V. Albano, J. Chem. Phys. **121**, 328 (2004).
[21] A. L. Barabasi and H. E. Stanley, *Fractal Concepts in Surface Growth* (Cambridge University Press, Cambridge, 1995).
[22] A. Bunde and S. Havlin, *Fractals and Disordered Systems* (Springer, Berlin, 1991).
[23] M. Rosso, J. F. Gouyet, and B. Sapoval, Phys. Rev. B **32**, 6053 (1985).
[24] M. Kolb and Y. Boudeville, J. Chem. Phys. **92**, 3935 (1990).
[25] J. W. Evans and T. R. Ray, Phys. Rev. E **50**, 4302 (1994); R. H. Goodman, D. S. Graff, L. M. Sander, P. Leroux-Hugon, and E. Clément, *ibid.* **52**, 5904 (1995).
[26] E. V. Albano, Physica A **216**, 213 (1995).
[27] N. Guisoni, E. S. Loscar, and E. V. Albano (unpublished).